Arabian Journal of Chemistry (2021) **14**, 103047

King Saud University

Arabian Journal of Chemistry

www.ksu.edu.sa
www.sciencedirect.com

ORIGINAL ARTICLE

Promotional effect of transition metals (Cu, Ni, Co, Fe, Zn)–supported on dolomite for hydrogenolysis of glycerol into 1,2-propanediol

Norsahida Azri [a,b], Ramli Irmawati [a,b,d,*], Usman Idris Nda-Umar [a,c], Mohd Izham Saiman [a,b], Yun Hin Taufiq-Yap [a,b,e]

[a] *Department of Chemistry, Faculty of Science, Universiti Putra Malaysia, 43400 UPM Serdang, Selangor, Malaysia*
[b] *Catalysis Science and Technology Research Centre (PutraCat), Faculty of Science, Universiti Putra Malaysia, 43400 UPM Serdang, Selangor, Malaysia*
[c] *Department of Chemical Sciences, Federal Polytechnic, PMB 55, Bida, Niger State, Nigeria*
[d] *Laboratory of Processing and Product Development, Institute of Plantation Studies, Universiti Putra Malaysia, 43400 UPM Serdang, Selangor, Malaysia*
[e] *Faculty of Science and Natural Resources, Universiti Malaysia Sabah, 88400 Kota Kinabalu, Sabah, Malaysia*

Received 5 October 2020; accepted 27 January 2021
Available online 3 February 2021

KEYWORDS

Transition metal;
Dolomite support;
Copper catalyst;
Acidity;
Glycerol hydrogenolysis;
1,2-Propanediol

Abstract Hydrogenolysis of biomass-derived glycerol is an alternative route to produce 1,2-propanediol. A series of transition metals supported on dolomite catalysts (Cu/Dol, Ni/Dol, Co/Dol, Fe/Dol, Zn/Dol) were prepared via impregnation, calcined at 500 °C and reduced at 600 °C. The synthesized catalysts were then characterized by BET, BJH, XRD, H_2-TPR, NH_3–TPD, and SEM, and subsequently evaluated in glycerol hydrogenolysis reaction to produce 1,2-propanediol (1,2-PDO). The nature of transition metals was found to influence the activation of the catalysts. Among the tested catalysts, copper supported on dolomite (Cu/Dol) exhibited appreciable hydrogenolysis performance due to the mutual interaction between the copper species and the dolomite. The findings from the various characterization results showed the addition of copper to dolomite ameliorates the chemical and reduction of the catalyst. It appears that the copper species were essentially enriched on the grain surfaces of the dolomite, the reduction properties, and the acidity of the catalyst enhanced. All the features of Cu/Dol catalyst contributed to the high glycerol conversion (78.5%) and high 1,2-PDO selectivity (79%) with low methanol production as the by-

* Corresponding author at: Department of Chemistry, Faculty of Science, Universiti Putra Malaysia, 43400 UPM Serdang, Selangor, Malaysia.
E-mail address: irmawati@upm.edu.my (R. Irmawati).
Peer review under responsibility of King Saud University.

Production and hosting by Elsevier

https://doi.org/10.1016/j.arabjc.2021.103047

product at 200 °C of reaction temperature, 4 MPa of reaction pressure and 10 h of reaction time.

1. Introduction

1,2-propanediol (1,2-PDO), also called propylene glycol (PG) is widely known as valuable chemicals used as monomer or additive in production of pharmaceuticals, cosmetics, solvent in food, as engine coolant, de-icing agent, and raw material for polyester resins (Gallegos-Suarez et al., 2015; Mauriello et al., 2015). Therefore, it has been regarded as a major commodity chemical with an estimated global production of about 1.4 million tons yearly at a 4% of annual market growth rate (Vasiliadou et al., 2011). The conventional production of 1,2-PDO is from petroleum derivatives via hydration process of hazardous propylene oxide (Bagheri et al., 2015; Rajkhowa et al., 2017). However, due to concern of petroleum shortage in the long-term, as well as the environment pollution issue, it is highly desirable to produce 1,2-PDO from a renewable source which may also substantially alters the price of 1,2-PDO. The surplus of glycerol as by-product from the rapid development of biodiesel (1 kg glycerol for every 9 kg biodiesel produced) could serve as an advantage and ideal solution for converting it into 1,2-PDO (Pandhare et al., 2016; Zhao et al., 2020). Due to above, the conversion of glycerol into 1,2-PDO via catalytic hydrogenolysis reaction has generated research interest. Generally, hydrogenolysis reaction require molecule bond dissociation and insertion of hydrogen into generated fragments which involve the cleavage of C-O bond of glycerol molecule while the C-C bond cleavage is undesired as it would lead to side products (Zheng et al., 2015). The evolution of 1,2-PDO from glycerol hydrogenolysis was described to proceed via dehydration of glycerol molecule to form acetol on acid site and further hydrogenation of acetol intermediate to 1,2-PDO on metal site (Balaraju et al., 2009, Mallesham et al., 2016, and Gandarias et al., 2012). The general reaction route for 1,2-PDO production is shown in Scheme 1.

Various heterogeneous catalysts have been well studied in glycerol hydrogenolysis, yielding different product compositions. In particular, the use of noble and lanthanide metals such as Pd, Pt, Ru and Ce have been reported with high selectivity to 1,2-PDO and high conversion of glycerol (Soares et al., 2016, Xia et al., 2011, and Yu et al., 2010). Alternatively, the use of transition metal-based catalysts such as Cr, Co, Ni, Cu, Zn and Zr, have also been associated with high catalytic activity. The transition metal-based catalysts were often preferred as a choice due to their efficiency towards C-O bond cleavage in contrast to C-C bond cleavage reaction (Freitas et al., 2018, Putrakumar et al., 2015, Zhao et al., 2020, and Mauriello et al., 2015). In addition, the lower price of transition metals in comparison to noble metals, emerge as the promising cost-effective substitute for noble metal as catalysts for hydrogenolysis of glycerol. However, the use of transition metal alone is of a big concern since metal leaching and sintering commonly occur. This is because the metal particles tend to aggregate under elevated reaction temperature due to a weak interaction among the metal species and thus easier to deactivate especially for a long reaction time thereby decreasing the catalytic performance (Wen et al., 2013). The presence of a support is highly desired in order to raise the activity and stability of the metal catalyst. The support behaves as a reservoir of spill over hydrogen that helps to hydrogenate surface species in which the available hydrogen from the support surface can pass to the surface metal and generate interfacial active reaction sites on metal-support surface and thus promote higher catalytic activity.

Substantial studies have been performed to probe the relationship between the catalytic reaction performance and the interaction of supports with catalyst metals of different nature. It is generally accepted that a combination of support and metal catalyst exhibit more attractive properties such as chemical and thermal strength, metallic phase stability, high metal dispersion and high metal reducibility. All these properties promote higher glycerol conversion and 1,2-PDO selectivity. Specifically, during glycerol hydrogenolysis, a catalyst support is supposed to be defined as a good reduction agent by the interaction of support and metal oxide. In this way, the reduction property of oxide species is enhanced. It has been reported that when a metal oxide is supported, the electrons from the support were directly transferred to the metal oxide species which then promote the formation of metallic species acting as active reaction sites for hydrogenation of C-O bond (Gallegos-Suarez et al., 2015). Due to the concern of good electronic properties, a metal catalyst is suggested to preferably interact with the oxide supports than the non-oxide supports such as carbon and polymeric resin.

In view of the above facts, thus supporting metal on a good support will no doubt improve catalyst efficiency in glycerol hydrogenolysis. In this study, dolomite with a mixture of mainly calcium carbonate ($CaCO_3$) and magnesium carbonate ($MgCO_3$) with several appreciable amount of SiO_2, Fe_2O_3, Al_2O_3 at ($< 5\%$) has been selected to be used as support in this work. Apart from its lower price, this support material has gained attention due to its acidic characteristics which are important in glycerol hydrogenolysis but the characteristic is rarely reported in literature. The presence of calcium and magnesium in dolomite may help in reducing metal oxides into metallic species since both metals have been identified as good reducing agents in electrochemical series. Incidentally, dolomite is abundantly available in Perlis, Malaysia and therefore can easily be accessible. Therefore, the objective of this research is to develop bifunctional supported metal catalysts comprising of acid and metal sites that possess good metal-support interaction species for high hydrogenolysis efficiency.

2. Experimental

2.1. Materials

In this study, the dolomite used as catalyst support was supplied by quarries in Chuping, Perlis Dolomite Industries, Malaysia. The metal precursors of copper nitrate hexahydrate

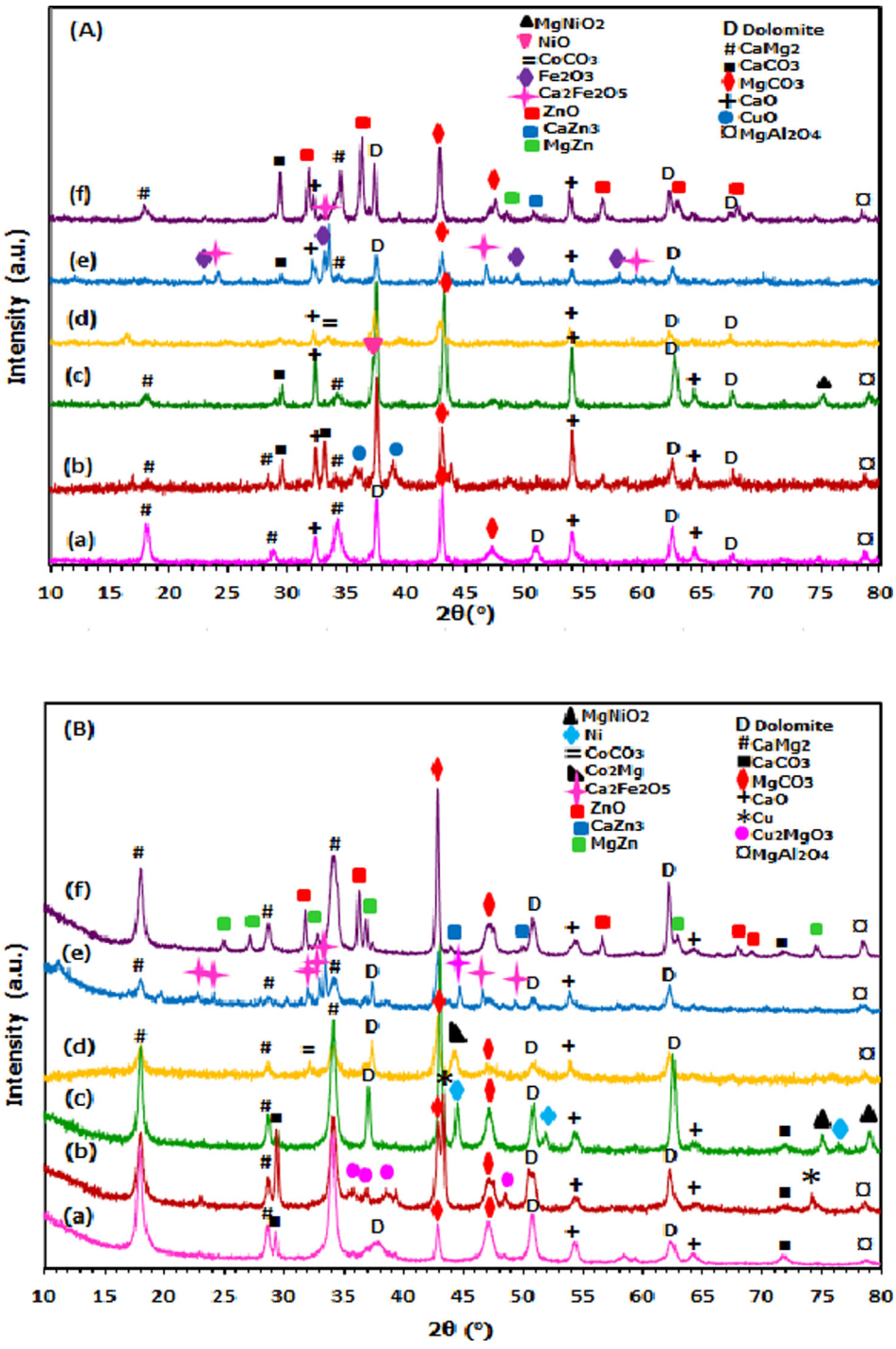

Scheme 1 Glycerol hydrogenolysis reaction pathway in acidic condition (Mallesham et al., 2016; Zhao et al., 2020).

$(Cu(NO_3)_2{\cdot}6H_2O)$ (≥99%), nickel nitrate hexahydrate (Ni $(NO_3)_2{\cdot}6H_2O$) (≥99%) and cobalt nitrate hexahydrate (Co $(NO_3)_2{\cdot}6H_2O$) (≥99%) were purchased from R&M Chemical Company, Malaysia. For iron nitrate nanohydrate ($Fe(NO_3)_3{\cdot}9H_2O$) (99%) and zinc nitrate hexahydrate ($Zn(NO_3)_2{\cdot}6H_2O$) (98%), the precursors were supplied from Bendosen Company. Glycerol (≥99.5%) was acquired from Sigma-Aldrich. All chemicals in this study were used as provided.

2.2. Catalysts preparation

Impregnation method was used in the production of all catalysts with a metal loading of 20 wt%. In a typical synthesis, 3.8 g of metal nitrate precursor was separately dissolved in 10 ml distilled water and was then poured into 4 g dolomite powder and was referred as supported metal catalyst denoted as M*/Dol (M = Cu/Ni/Co/Fe/Zn). The mixture was then

stirred using magnetic stirrer at 300 rpm and further dried for 3 h with heating at 90 °C on a hot plate. The dried mixture was then aged in drying oven for 24 h at 120 °C. After that, the synthesized catalyst was charged for calcination at 500 °C for 3 h in a tube furnace under static air with ramping of 10 °C/min in order to remove all the nitrate salt present in the catalysts. The calcined catalysts were then reduced by 5% H_2/Ar at 600 °C for 3 h at a heating rate of 2 °C/min in the same tube furnace. All the synthesized catalysts were used as such for glycerol hydrogenolysis reaction.

2.3. Catalyst characterization

The textural properties of catalysts were determined from the adsorption–desorption isotherms of nitrogen using Gemini apparatus (Micromeritics 2010 Instrument Corporation). Prior to measurements, the catalyst sample was degassed at 150 °C for 24 h in order to remove all the moisture and foreign gases deposited on the catalyst surface. Then the adsorption and desorption processes of N_2 was then analyzed in a vacuum chamber at −196 °C. The catalyst surface area was determined by Brunauer-Emmett-Teller (BET) method while the pore size distribution was calculated using the method of Barrett, Joyner and Halenda (BJH).

The X-ray diffraction (XRD) analysis was performed in order to analyse the phase composition structure of the crystalline catalysts and its crystallite size. It was conducted using a Shimadzu diffractometer model XRD-6000 by employing CuK_α radiation source with wavelength of $\lambda = 0.1541$ nm, generator current of 30 mA and voltage of 40 kV. The finely ground samples were scanned at a speed of 2°/min using a Siemens D-500 diffractometer and the corresponding diffractogram data were collected from scattering angles at range $2\theta = 10–80°$ while phase identification was determined by matching experimental patterns with the JCPDS diffraction file. The crystallite size (nm) of the catalyst particle was calculated using Debye-Scherrer equation corresponding to full width of half maximum (FWHM) of respective peak.

The characteristic of metal reducibility was measured by temperature-programmed reduction (H_2-TPR), using Thermo-Finnigan TPD/R/O 1100 SERIES equipped with a TCD (thermal conductivity detector). In a typical experiment, the amount of hydrogen consumption was initially calibrated using known amount of CuO powder as reference standard by pulse chemisorption technique in order to ensure the sensitivity of thermal conductivity detector (TCD) signal. The H_2 consumption generated from the calibration of CuO powder was calculated and the value was set as a calibration factor to calculate the H_2 uptake for the next analysis. Prior to sample analysis, catalyst sample (~0.05 g) was pre-treated for removing moisture content using N_2 flow at a heating of 120 °C for 30 mins (at a rate of 20 cm^3/min) before cooling down to room temperature. After the catalyst pretreatment, an in-situ H_2 chemisorption analysis was performed from 50 to 1000 °C for 1 h (10 °C/min) in 5% H_2/Ar (25 cm^3/min). Thereafter, the data from reduction of chemisorbed sample was measured from the generated peak area of hydrogen consumption.

The acid sites distribution and total acidity amount of catalyst were studied by temperature programmed desorption of ammonia (NH_3-TPD) (Thermo-Finnigan TPD/R/O 1100 SERIES). Before sample analysis, the TCD signal was initially calibrated using known amount of CuO powder as reference standard. The generated NH_3 concentration was then referred as calibration factor value for the next sample analysis. As for sample analysis, catalyst sample (~0.05 g) was initially carried out with ammonia adsorption in ammonia flow at room temperature for 1 h. Thereafter, the adsorbed ammonia was desorbed at 50–1000 °C in helium flow (30 cm^3/min) and with heating rate of 10 °C/min. The total acidity amount of the catalyst was determined by the integration of peak area (area under graph) of the analyzed sample.

The morphological characteristic of all the catalysts were acquired using scanning electron microscopy (SEM) using an apparatus from Rayny EDX-720. During the analysis, the surface images of a catalyst were spotted through LEO 1455 VP electron microscope in a high-vacuum condition at 20 kV.

2.4. Reaction set up for glycerol hydrogenolysis

The catalytic tests were conducted in a 150 ml stainless steel autoclave reactor (SS316L series) equipped with Teflon lining cup, an electrical heating jacket and a magnetic stirrer. In a typical experiment, the autoclave reactor was charged with 4 g glycerol solution, 16 g distilled water, and 1 g synthesized catalyst. The reactor then was purged and pressurized with H_2 to the desired pressure. Afterwards, the reactor was heated in a defined reaction time for hydrogenolysis reaction. During the catalytic reaction, the reactor was set at maximum H_2 pressure, temperature and time of 4 MPa, 200 °C and 10 h, respectively. For all catalytic reactions, the reactor was left stirred at 400 rpm. The reaction starting time was defined once the reactor temperature reached the desired reaction temperature. After completion of the reaction, the reactor was cooled down to room temperature, and the obtained liquid product was collected and separated from the catalyst by centrifugation process at 3000 rpm for 15 min. For comparison study, a blank reaction (reaction being conducted without the presence of any catalyst powder and/or support) was also performed under similar reaction parameters.

2.5. Product analysis

The obtained liquid product from glycerol hydrogenolysis reaction was analyzed using gas chromatography-flame ionization detector (GC-FID) equipped with HP-5 capillary column (length: 30 m × inner diameter: 0.32 mm × film thickness: 0.25 μm). It was operated at 300 °C with splitless inlet mode. Prior to analysis, the liquid product was extracted using ethyl acetate in a 1:1 ratio. The extraction was carried out three times. Subsequently, the product solution was dried in oven at 70 °C for 15 mins in order to concentrate the solution. Lastly, a derivatization process was charged to the liquid sample before it is being analyzed by GC analysis. Typically, *N-O*-bis(trimethylsilyl)trifluroacetamide (BSTFA) was used as the silyl agent and was mixed with pyridine (C_5H_5N) as binding solvent in a 1:1 ratio and was then left dried in oven for 20 mins at 60–70 °C so as to achieve complete silylation process. 1 μL amount of the derivatized product was directly injected to GC. The initial temperature was determined at 40 °C and held for 6 min with rate of 7 °C min^{-1} towards reaching the final temperature of 270 °C. The temperature for injection was set at 250 °C. The glycerol conversion and the selectivity of

product were acquired by comparing the retention time of standard with the obtained experimental-based products on GC chromatogram peak. The equations for calculation of glycerol conversion and 1,2-PDO selectivity are depicted in Equation (1.1) and Equation (1.2), respectively.

$$\text{Glycerol conversion, } \% = \frac{C_{glycerol,in} - C_{glycerol,out}}{\sum C_{glycerol,in}} \times 100\% \quad (1.1)$$

$$1,2-PDO\ selectivity, \ \% = \frac{C_{1,2-PDO}}{[C_{Total}]} \times 100\% \quad (1.2)$$

Where, $C_{glycerol,in}$ is described as the initial concentration of glycerol and $C_{glycerol,out}$ as the final concentration of glycerol. And C_{total} is the sum of the product detected in the liquid product. (All peaks regarded to the product in this study were confirmed by the peak of standard solution)

3. Results and discussion

3.1. Textural properties

The textural properties of all catalysts derived from N_2 adsorption–desorption isotherms are presented in Table 1. The BET specific surface area of dolomite, Cu/Dol, Ni/Dol, Co/Dol, Fe/Dol and Zn/Dol, were found to be 13.3, 9.7, 3.5, 7.8, 2.1 and 2.9 m^2g^1, respectively. The decreasing surface area of supported metal oxide samples as opposed to dolomite was due to the filling of metal oxide in the support pores. This finding was similar to Thirupathi et al. (2012), who stated that the reduction in the surface area of Mn–Ni(0.4)/TiO_2 catalyst was due to the blocking effect of the loaded nickel oxide on the support material. The decrease of catalyst's surface area was consistent with the catalyst pore volume which shows decrease from 0.276 cm^3g^{-1} (dolomite) to 0.096, 0.071, 0.145, 0.037, 0.073 cm^3g^{-1} for Cu/Dol, Zn/Dol, Co/Dol, Fe/Dol and Ni/Dol catalyst, respectively. This behavior was due to the blockage and destruction of the catalyst structure similar to the report of Zhao et al. (2013).

Similarly, different supported metal catalysts exhibited different pore diameter ranging from 19.04 Å to 156.34 Å. Cu/Dol, Fe/Dol and Zn/Dol catalysts showed smaller pore diameter in the range 19.07–27.82 Å compared to that of dolomite support (152.02 Å) while Ni/Dol and Co/Dol catalyst presented bigger pore diameter of 155.90 Å and 156.34 Å, respectively. It is worth mentioning that the Cu/Dol, Fe/Dol and Zn/Dol catalysts exhibited both smaller in pore diameter and pore volume of (0.098 cm^3g^{-1} and 19.07 Å), (0.037 cm^3g^{-1} and 19.04 Å) and (0.071 cm^3g^{-1} and 27.82 Å), respectively than dolomite support (0.276 cm^3g^{-1} and 152.02 Å). The small pore diameter and pore volume of those catalysts could be related to the occurrence of new active sites (new pore) formed on the catalyst surface. This characteristic is somehow an advantage because it would reduce the metal species from being easily leached. This consequently may lead to the stronger adsorption–desorption of the active sites during catalytic reaction. Also, the presence of active sites inside the small pore was assumed to help in the reusability and stability for the next reaction cycle.

Meanwhile, the N_2 adsorption–desorption isotherms and pore size distribution curves of all catalysts are compiled in supplementary material (Fig. S-1 and Fig. S-2). It shows the type III isotherm for dolomite support and all supported metal catalysts. This isotherm was assigned to the weak interaction characteristic of multilayer adsorption of typically clustered catalyst material. Furthermore, the similar isotherm of dolomite support and supported metal catalysts suggesting that the dolomite structure was not significantly modified even with addition of metals. The formation of hysteresis $p/p^\circ > 0.8$ was observed, which showed a characteristic of typical non-rigid aggregates of plate-like particles (slit pore shape) with non-uniform size of the catalyst (Luna et al., 2018). Meanwhile, the isotherms for dolomite support exhibited lower N_2 adsorbed volume (~1 cm^3g^{-1}) than supported metal catalysts, indicating the macroporous characteristic in the catalyst material. The higher N_2 adsorbed volume exhibited by supported metal catalysts could be corresponded to the presence of some mesopores. The distribution of pore size curve of all catalysts obtained by Barrett, Joyner, and Halenda (BJH) method shown in Fig. S-2 revealed that the pore size distributions of dolomite, Cu/Dol and Ni/Dol catalysts were in range 2 to 50 nm. On contrary to the Co/Dol, Fe/Dol and Zn/Dol catalysts, the pore sizes were in range 1–90 nm.

3.2. XRD analysis

The XRD diffractograms of calcined and reduced samples are presented in Fig. 1(A) and Fig. 1(B), respectively. The XRD pattern of dolomite support was observed with mixed crystalline phases. The diffraction peaks at $2\theta = 18.1^\circ$, 28.3°, and 33.8° were assigned to $CaMg_2$ (JCPDS; 01–1070). The peaks at $2\theta = 37.51^\circ$, 50.76°, and 62.20° were due to dolomite phase (JCPDS; 02–0767) while two peaks at $2\theta = 44.2^\circ$ and 47.4° were denoted as $MgCO_3$ phase ((JCPDS; 02–0871). The presence of CaO phase shows peak at $2\theta = 32.4^\circ$ and

Table 1 Surface and textural properties of catalysts.

Catalyst	BET surface area (m^2g^{-1})	Pore Volume (cm^3g^{-1})	Pore diameter (Å)	Crystallite size (nm)[a]
Dolomite	13.3	0.276	152.02	27.44
Cu/Dol	9.7	0.098	19.07	54.80
Ni/Dol	3.5	0.073	155.90	34.32
Co/Dol	7.8	0.145	156.34	22.87
Fe/Dol	2.1	0.037	19.04	19.60
Zn/Dol	2.9	0.071	27.82	22.87

[a] The data were estimated according to the Scherrer equation using the FWHM of the dolomite peak at $2\theta = 62.45^\circ$.

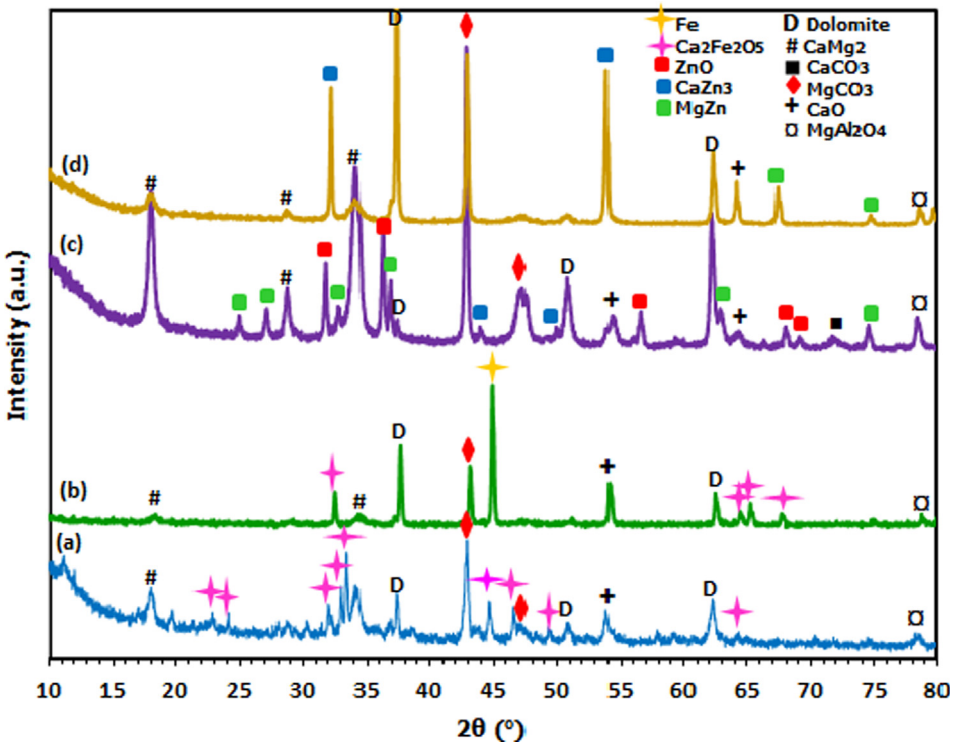

Fig. 1 XRD diffractograms of calcined (A) and reduced samples (B) of (a) Dolomite, (b) Cu/Dol, (c) Ni/Dol, (d) Co/Dol, (e) Fe/Dol and (f) Zn/Dol catalyst.

54.2° (JCPDS; 01–1160) and the less intense peak for $MgAl_2O_4$ phase was detected at 2θ = 78.7° (JCPDS; 03–1160). These phases are also present in all supported metal catalysts but with reduced peak intensities as a consequence of the embedment of metal oxides in the dolomite matrix. In return new phases corresponded to the respective metal oxide were seen such as CuO at 2θ = 35.5° and 38.8° (JCPDS; 44–0706), NiO at 2θ = 37.2° (JCPDS; 01–1239), Fe_2O_3 at 2θ = 23.7°, 34.1°, 50.1° and 58.2° (JCPDS; 02–0915) and ZnO at 2θ = 3 2.5°, 36.5°, 56.8°, 68.3° and 69.7° (JCPDS; 03–0888).

Nevertheless, in the case of Co/Dol catalyst, no characteristic peak of CoO phase was detected, instead cobalt carbonate ($CoCO_3$) was formed at 2θ = 34.1° (JCPDS; 01–1020). Apart from that, an alloy phases were also detected with the presence of $MgNiO_3$ spinel (JCPDS; 03–0999) at 2θ = 75.2°, $Ca_2Fe_2O_5$ spinel (JCPDS; 02–0936) at 2θ = 24.8°, 34°, 45.5° and 60.1°, MgZn (JCPDS; 08–0206) and $CaZn_3$ (JCPDS; 35–1159) at 2θ = 50.2° and 2θ = 53.5°, respectively. On the other hand, it was noted that there was no characteristic peak related to any metallic species was observed in all calcined samples.

The XRD patterns of the reduced catalysts in Fig. 1(B) shows that the intensity of diffraction peak at 2θ = 43.5° corresponded to $MgCO_3$ phase of all supported metal catalysts became more intense and higher upon the addition of respective metal to dolomite support. This is due to the interaction of metal species with dolomite support. For reduced dolomite, apart from peaks presented in calcined dolomite, new peaks were also detected such as $CaCO_3$ at 2θ = 29.3° and 72.2° (JCPDS; 01–1032). For supported metal catalysts, it was displayed that upon reduction by H_2 at 600 °C, the diffraction peaks of CuO (2θ = 35.5°, 38.8°) and NiO (2θ = 37.2°) of Cu/Dol and Ni/Dol catalysts disappeared, while the characteristic peaks attributed to metallic Cu species (2θ = 43.5° and 74.1°) (JCPDS; 085–1326) and metallic Ni species (2θ = 44. 2°, 52.1° and 76.1°) (JCPDS; 001–1260) were emerged. Similar diffraction peaks of metallic copper and nickel was also reported by Wen et al. (2013) and Srivastava et al. (2017). Additionally, it was found that no characteristic peak attributed to any Cu_2O and Ni_2O phases was detected in Cu/Dol and Ni/Dol catalysts, indicating the reduction of Cu^{2+} and Ni^{2+} species was complete (Zhu et al., 2013, Zhao et al., 2013and Gandarias et al., 2012). The presence of metallic Cu and Ni species are regarded as active reaction site for the catalytic reaction and thus could increase the glycerol hydrogenolysis reaction.

The presence of Cu^0 and Ni^0 species was attributed to their high reduction ability from metal oxides-dolomite interaction. It could be suggested that the migration of electron (oxidation and reduction) happened on metal oxide-support surface via electrons lone pair would cause the destabilization of metal oxide bond and thus promote the reducibility of oxides (Nagaraja et al. 2007). In this present work, the CaO, $CaMg(CO_3)_2$ and $MgCO_3$ species were suggested to be the one involved for the copper and nickel oxide reduction since calcium and magnesium has been identified as good reducing agent (Tasyurek et al., 2018).

Accordingly, it has been revealed that metal oxide species was prone to generate spinel when it was supported with clay or limestone material containing Mg and Ca (Kovanda et al., 2001; Pardeshi et al., 2010). Apparently, the Cu_2MgO_3 (2θ = 35.3°, 37.5°, 38.2° and 48°), $MgNiO_2$ (2θ = 75.3° and 79.2°) and ($Ca_2Fe_2O_5$) (2θ = 23°, 24°, 32°, 33°, 34°, 44°, 47° and 49°) phases were detected for Cu/Dol, Ni/Dol and Fe/Dol catalysts, respectively, thereby confirming the formation of metal

species in spinel. For Co/Dol and Zn/Dol catalysts, alloy phases of Co_2Mg and ($CaZn_3$, MgZn) were detected. Notably, no characteristic peak of any metallic Co, Fe, and Zn species was observed in Co/Dol, Fe/Dol, and Zn/Dol catalysts possibly due to the incomplete H_2-reduction of the catalysts. In particular for Zn/Dol catalyst, ZnO phases was obviously seen, indicating higher reduction temperature is required to transform the oxide phase into metallic species.

The dolomite's crystallite size was estimated from the XRD peak by choosing $2\theta = 62.45$ and the results are summarized in Table 1. The dolomite's crystallite size was found increases when Ni and Cu were supported on it. The trend of crystallite size ranks as Cu/Dol > Ni/Dol > Dol > Co/Dol ≈ Zn/Dol > Fe/Dol. The larger crystallite size of Cu/Dol and Ni/Dol than dolomite probably attributed to the metal species which occupied in the interstitial support bulk thus increased the catalyst crystal size. This could also be correlated to the non shifted peak of $MgCO_3$ phase at $2\theta = 43.5°$, with respect to dolomite support. The non shifted peak reflected to the presumption that metal promoter was incorporated well on the support (Asikin et al., 2017). However in the case of Co/Dol, Fe/Dol and Zn/Dol catalysts, the dolomite's crystallite size were decreased from 27.4 nm to 22.9 nm, 19.6 nm, and 22.9 nm, respectively, indicating Co, Fe and Zn species were prone to dissolve in the support lattice as substitutional metal rather than occupied in the interstitial support lattice (Liu et al., 2014). The presence of substitutional metal could be also corresponded to the shifted peak of $MgCO_3$ phase at $2\theta = 43.5°$ to slightly lower degree than dolomite peak.

In the case of Fe/Dol and Zn/Dol catalysts, a higher reduction temperature of 900 °C was applied to reduce both oxide species into their metallic form and the XRD patterns are depicted in Fig. 2. The results obtained were compared with the previous catalysts reduced at 600 °C. It can be seen that the characteristic peak of metallic Fe (JCPDS; 01–1267) was clearly appeared at $2\theta = 44.8°$ indicating that the reduction temperature of 900 °C successfully reduced iron oxide to its metallic species. Meanwhile the formation of $Ca_2Fe_2O_5$ spinel was also noticeable. Nevertheless, it was observed that the presence of $Ca_2Fe_2O_5$ spinel became gradually invisible as compared to 600 °C reduced sample which suggested that the spinel species was also reduced at higher temperature.

In the case of Zn/Dol catalyst, no characteristic peak attributed to metallic Zn species was detected even after reduction at 900 °C, rather the presence of alloy phase ($CaZn_3$ and MgZn). This indicates that reduction at 900 °C was still not able to transform Zn oxide into its metallic form. However, it was noticed that the diffraction peaks of ZnO phase at $2\theta = 32.5°$, 36.5°, 56.8°, 68.3° and 69.7° disappeared, while $CaZn_3$ and MgZn phases at ($2\theta = 32.5°$ and 54.5°) and ($2\theta = 68.5°$ and 75.5°), respectively became more intense peak. This finding is in good agreement with the work of Consonni et al. (1999), who investigated the reduction property of Pt/ZnO catalyst and found that the reduced ZnO catalyst had resulted to the formation of PtZn alloy instead of metallic Zn species.

3.3. H_2-Temperature programmed reduction (H_2-TPR)

The H_2-TPR profiles of dolomite and supported metal catalysts (Cu/Dol, Co/Dol, Zn/Dol, Ni/Dol and Fe/Dol) are depicted in Fig. 3(A) while the corresponding hydrogen consumption data is tabulated in Table 2. From TPR profiles, it was discovered that Cu/Dol and Co/Dol catalysts gave a lower reduction peaks as opposed to dolomite support at 689 °C. The reduction of Cu/Dol and Co/Dol was assigned at (291, 455 and 630 °C) and (435 and 638 °C), respectively. Apart from that, it is worthy to note that, the reduction peak of all supported metal catalysts was found to emerge broader and higher than dolomite due to the species reduction from metal alloy phases thereby consumed higher hydrogen adsorption and hence enlarged the reduction peak (Li et al., 2009). Similar behavior was outlined by Soares et al. (2016a,b), the authors indicated that the broader reduction range was detected after addition of Cu to Ru/ZrO_2 catalyst which caused interphase hydrogen adsorption of the metals (slow adsorption) due to metal cluster formation from Ru and Cu alloys.

According to Zhao et al. (2017), the reduction of dispersed copper oxide species to metallic copper (Cu^0) was effective at < 250 °C. Smaller catalyst particles reduce faster when compared with that of CuO in bulk (Zhu et al., 2013). Correspondingly, the reduction of bulk CuO phase took place at temperature higher than 250 °C (Wen et al., 2013). According to Vargas-Hernandez et al. (2014), reduction at > 400 °C was due to the metal-support species or copper in spinel phase. Tanasoi et al. (2009) reported that the Cu-containing mixed oxide reduced at range 400–750 °C due to the presence of complex copper phases of $CuAl_2O_4$ and $Cu_xMg_xAl_2O_4$. Therefore, in this study, the first two reduction profiles of Cu/Dol catalyst were assigned for reduction of CuO to metallic Cu. Peak at 291 °C corresponded to the reduction of small and big clusters of CuO to metallic copper (Cu^0) while peak at 455 °C attributed to the reduction of copper oxide in interstitial defects in dolomite crystalline phase since Cu_2MgO_3 was previously detected by XRD peak. Reduction of CuO corresponded to two reduction steps of Cu^{2+} ions to Cu^+ ions ($CuO \rightarrow Cu_2O$), followed by reduction of Cu^+ ions to metallic copper ($Cu_2O \rightarrow Cu^0$). Peak maximum at 630 °C was ascribed to reduction of dolomite because the peak profile was close to that of bulk dolomite (639 °C).

As for Co/Dol catalyst, it was reported that the reduction temperature of CoO to Co was occurred below 400 °C (Yan et al., 2011). Thus, peak at 435 °C could be referred to reduction of cobalt species from $CoCO_3$ phase as presented in XRD profile in Fig. 1(B). The presence of metallic cobalt species was not noticed in XRD profile probably due to well dispersed metallic Co species or with minor proportion, rather the formation of $CoMg_2$ phase was observed. Apart from that, the formation of $CoCO_3$ peak was still detected in the reduced catalyst. This shows that cobalt species in the form of carbonate was not easily reduced at 600 °C. As stated in literature, the reduction cobalt oxide depends on the cobalt particle size and the properties of the support used (Yan et al., 2011). The presence of broad peak at 638 °C could be due to the reduction of cobalt species which strongly interacted with support. From this study, the high metal reducibility and lower reduction temperature of Cu/Dol and Co/Dol catalysts could be due to the good electronic interaction of Cu and Co oxide with calcium and magnesium species from dolomite.

For Ni/Dol, Fe/Dol and Zn/Dol catalysts, higher reduction temperature was observed at (690 and 962 °C), (646 and 946 °C) and 700 °C, respectively. In the case of Ni/Dol catalyst, the broader and higher peaks at 690 °C and 962 °C than that of dolomite peak could be attributed to the reduction of

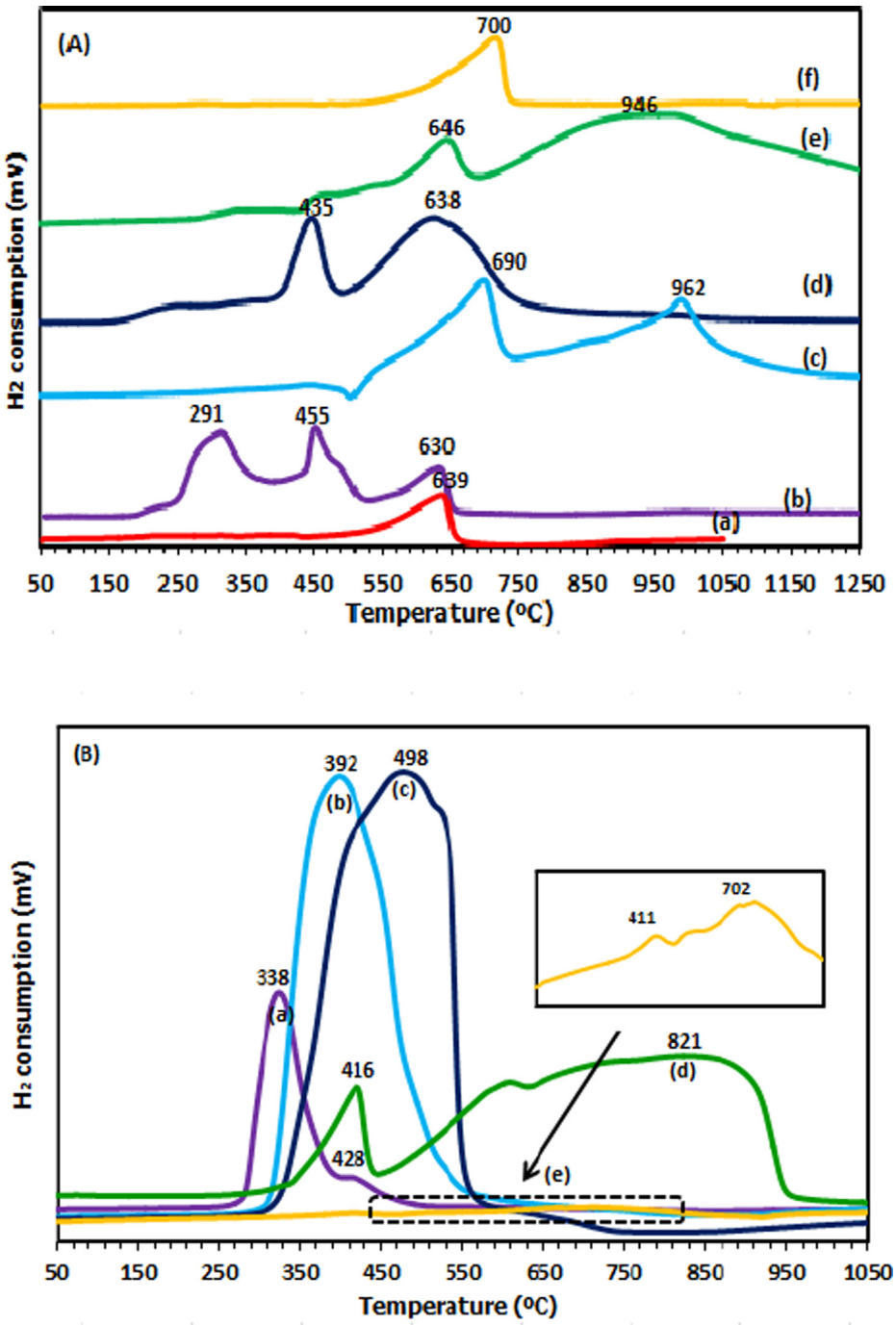

Fig. 2 XRD diffractograms of reduced samples of (a) Fe/Dol (600 °C), (b) Fe/Dol (900 °C), (c) Zn/Dol (600 °C) and (d) Zn/Dol (900 °C).

nickel and dolomite species which had stronger metal-support interaction or attributed to the reduction $MgNiO_2$ phase. Similar results were proposed by Srivastava et al. (2017), who stated that the broad peak and high reduction temperature of Ni/Al_2O_3 catalyst was due to the reduction of NiO species which was in intimate contact with Al_2O_3 support and/or attributed to the reduction of $NiAl_2O_4$ phase. For Fe/Dol catalyst, peak at 646 °C was attributed to the reduction of dolomite. Peak at 946 °C was ascribed to the reduction of iron species in $Ca_2Fe_2O_5$ spinel phase which strongly interacted with dolomite. In the case of Zn/Dol catalyst, peak at 700 °C could most likely be related to the reduction of dolomite with zinc species from $CaZn_3$ and MgZn alloys. On a general note, Cu/Dol catalyst could be proposed to predominantly exhibit higher metal reducibility than Co/Dol due to its lower reduction temperature. The presence of metallic Cu in XRD peak agreed well with its high reduction character. This observation provided the bases for conducting the hydrogenolysis of glycerol

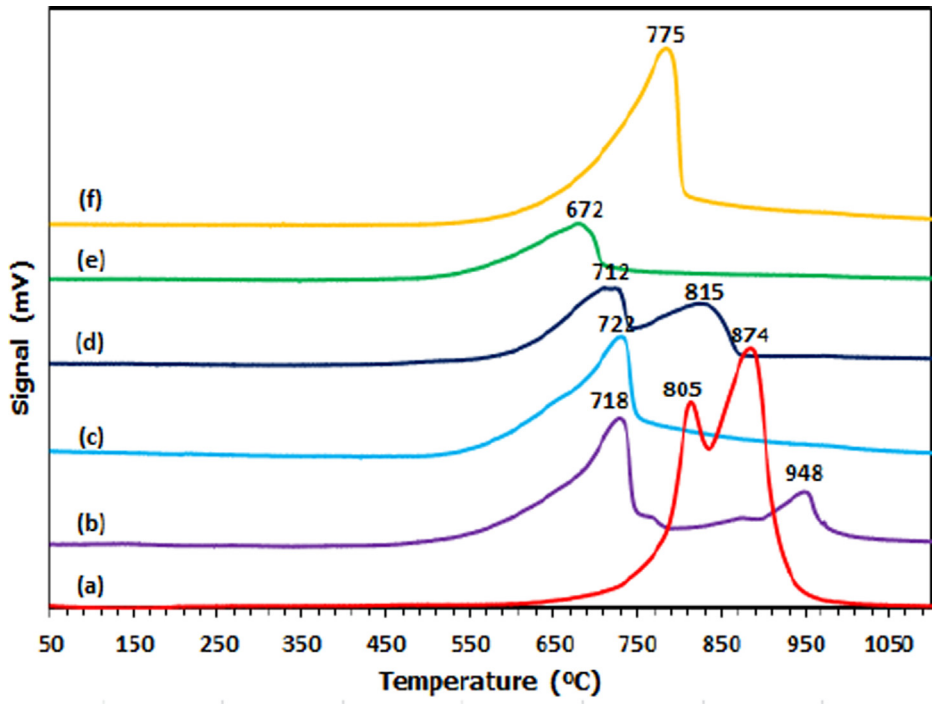

Fig. 3 H_2-TPR profiles of (A) for (a) Dolomite, (b) Cu/Dol, (c) Ni/Dol, (d) Co/Dol, (e) Fe/Dol, (f) Zn/Dol catalyst while (B) for (a) Copper oxide, (b) Nickel oxide, (c) Cobalt oxide, (d) Iron oxide and (e) Zinc oxide.

Table 2 Reducibility data of catalysts.

Catalyst	H_2 consumed at different temperatures[a] (μmol/g)		Total amount H_2 consumption for all species (μmol/g)	Reduction degree (%)[b]
	150–550 °C	> 550 °C		
Dolomite	–	1005	1005	–
Cu/Dol	23582, 17919	10268	51769	> 100
Ni/Dol	–	30657, 40691	71348	> 100
Co/Dol	19250	54712	73962	> 100
Fe/Dol	–	10131, 47852	57983	> 100
Zn/Dol	–	14955	14955	> 100
Copper oxide	110	–	110	13.9
Nickel oxide	120	–	120	14.1
Cobalt oxide	47	–	47	5.5
Iron oxide	39	120	159	17.8
Zinc oxide	189	740	193	25.2

[a] H_2-TPR consumption peak for all catalysts.
[b] Reduction degree = (H_2 consumption by TPR/theoretical H_2 consumption) × 100%, assuming $M^{2+} + H^2 \rightarrow M^0 + 2H^{2+}$.

reaction at 200 °C since the presence of active reaction sites (metallic copper species) would be preserved and thus stable during the catalytic reaction.

From Table 2, it was observed that the total hydrogen consumption of all supported metal catalysts was higher than that of dolomite following this trend Co/Dol > Ni/Dol > Fe/Do l > Cu/Dol > Zn/Dol > Dol. This finding could be correlated to a study reported by Zhao et al. (2019) who stated that the total amount of H_2 consumed for CuO/CeO_2 catalyst was far exceeded than that necessary for the complete reduction of pure CuO, specifying that some ceria support would be involved during the reduction process. In this study, the addition of respective metal to dolomite support influenced catalyst reducibility due to higher species exposure area and thus elevates the hydrogen consumption amount. Mallesham et al. (2016) and Gandarias et al. (2012) proposed that when a support was promoted by reducible metal oxide, the availability of hydrogen to be consumed was enhanced as well as the catalytic hydrogenation of alcohol. The presence of $CaCO_3$, $MgCO_3$, CaO and $MgAl_2O_4$ phases from dolomite could be considered to provide a source of chemisorbed hydrogen atoms and increased the amount of hydrogen uptake.

Additional analysis of metal oxides reduction was carried out as shown in Fig. 3(B) while the corresponding hydrogen

consumption data is given in Table 2. It can be seen that copper oxide shows the lowest reduction temperature at 338 and 428 °C, while the reduction peak for nickel oxide was appeared at 392 °C. The peak for cobalt oxide and iron oxide was at 498 °C and (416 °C and 821 °C), respectively. In the case of zinc oxide, the reduction profile was rather flat and the blow-up image shows peaks at 411 °C and 702 °C. Comparing the reduction profiles of both Cu and Co oxides with that of the supported metal catalysts, the later gave a lower reduction peaks. This confirms that the reducibility of those oxide species in supported catalysts was enhanced which due to the promotional effect of metal oxide-dolomite interaction. On the other hand, the reduction of nickel oxide, iron oxide and zinc oxide was noticed far from the reduction region of their supported metal catalysts. This confirms the poor metal reducibility of their oxides. From Table 2, it was demonstrated that the H_2 consumption needed for the complete reduction of metal oxides was in range 47–929 μmol/g which was obviously far less than the amount required for supported metal catalysts (14955–73962 μmol/g). Thus, it was suggested that the capability for hydrogen consumption was enhanced in the case of metal oxide supported on dolomite.

3.4. Ammonia temperature programmed desorption (NH_3-TPD) analysis

The available acid sites of dolomite and all supported metal catalysts were performed via NH_3-TPD. The classification of acid strength was interpreted as weak (< 250 °C), medium (250–500 °C) and strong (> 500 °C) (Srivastava et al., 2017). The desorption profiles of all catalysts are indicated in Fig. 4 while the corresponding acidity (amount of ammonia uptakes) is tabulated in Table 3. All catalysts exhibited desorption peaks above 500 °C, indicating the presence of strong acid sites on the catalyst surface. In all supported metal catalysts, the presence of desorption peaks showed rather smaller and lower desorption profile than dolomite support. Cu/Dol catalyst appeared with higher desorption temperature (at 948 °C) than dolomite (at 874 °C) and other supported catalysts. Dolomite showed two desorption peaks at 805 °C and a shoulder at

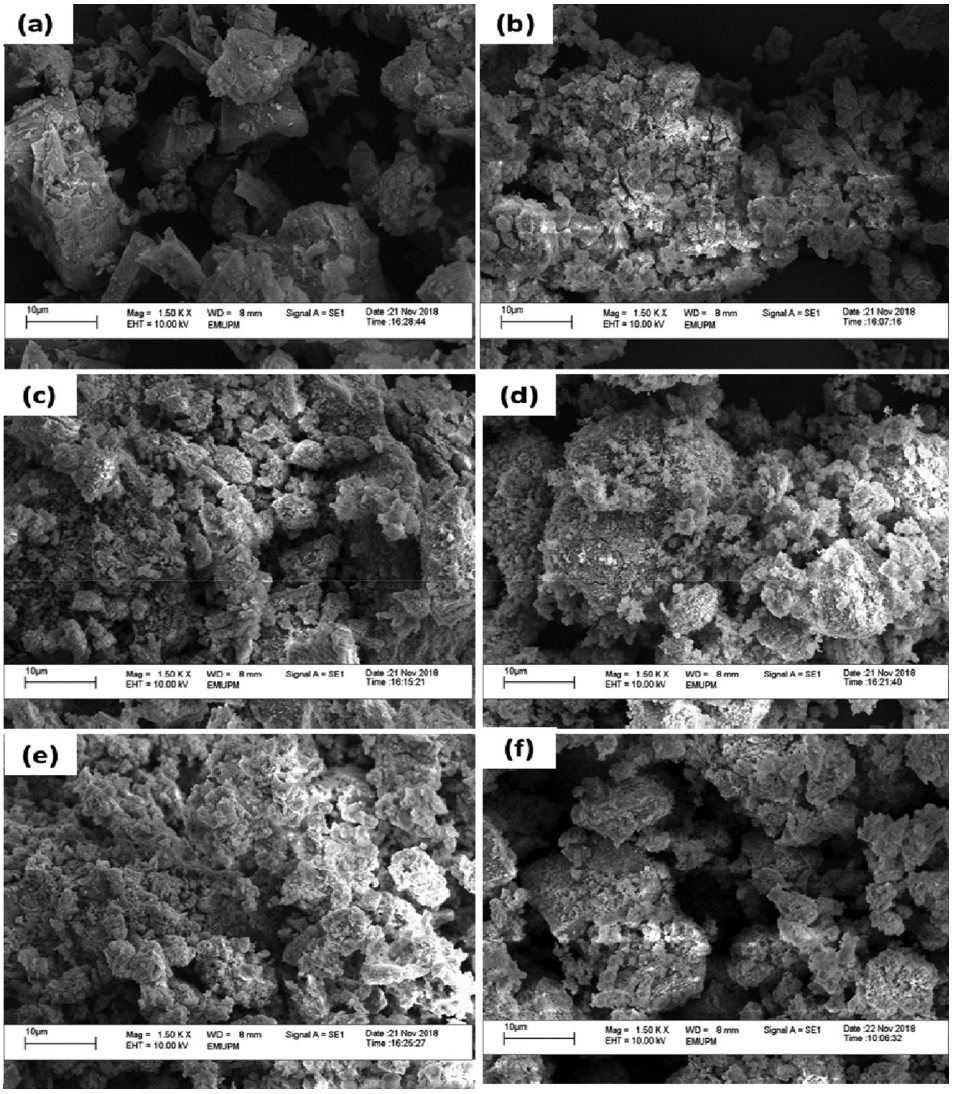

Fig. 4 NH_3-TPD profiles of (a) Dol, (b) Cu/Dol, (c) Ni/Dol, (d) Co/Dol, (e) Fe/Dol and (f) Zn/Dol.

874 °C. For Cu/Dol and Co/Dol catalysts, two desorption peaks emerged at (718 and 948 °C) and (712 °C and 815 °C), respectively. In the case of Ni/Dol, Fe/Dol and Zn/Dol, only one desorption peak appeared which at 722 °C, 672 °C and 755 °C, respectively.

Notably, the desorption peak of supported metal catalysts with the exception of Cu/Dol shifted towards lower desorption temperature than dolomite from 805 to 874 °C (dolomite) to 672–815 °C (supported metal catalysts). In the case of Cu/Dol, the second desorption peak was shifted to 948 °C (Cu/Dol), indicating the presence of much stronger acid sites in the catalysts. This attributable to the strong interaction of copper on the dolomite support and a sign that copper was well incorporated and dispersed over dolomite surface than other catalysts. The acidity data in Table 3 shows that the addition of respective metal promoter to dolomite support contributed to different acid amount. Incorporation of nickel, cobalt and iron, gave a decrease in the acidity from 16149 μmol/g (dolomite) to 14305, 11172, 6075 μmol/g for Ni/Dol, Co/Dol and Zn/Dol catalyst, respectively. This could be assigned to the coverage of the metal species (Ni, Co and Fe) on dolomite surface, therefore allowed limited accessibility of NH_3 gas to be bonded with the catalyst pore. This finding was in agreement with the work of Priya et al. (2017), who proposed the decrease of acid amount in metal-promoted mordenite catalyst was attributed to the blockage caused by the metal species. In another study reported by Vasilidiaou et al. (2009), it claimed that the decrease in catalyst acidity of Ru-supported catalyst was due to the Ru species was possibly reside (occupied on the alumina support surface).

On the contrary, when copper and zinc was added to dolomite support, the acidity was increased from 16149 μmol/g (dolomite) to 19528 μmol/g (Cu/Dol) and 17085 μmol/g (Zn/Dol), respectively. The similar behavior was also reported by Thirupathi et al. (2012), where the addition of nickel species on Mn/TiO_2 catalyst improved and broadened the acid site distribution of the catalyst. The order of catalyst acidity ranks as Cu/Dol > Zn/Dol > Dol > Ni/Dol > Co/Dol > Fe/Dol. It should be noted that the high acid sites of Cu/Dol and Zn/Dol catalysts could act as active reaction sites which contribute to high reactivity of C-O bond cleavage of glycerol molecule during dehydration step and consequently enhance the catalytic reaction of glycerol hydrogenolysis to a higher level. The presence of carbonate phases ($CaCO_3$, $MgCO_3$) in dolomite could be the one responsible to provide a source of chemisorbed NH_3 gas and increase catalyst acidity of Cu/Dol and Zn/Dol catalysts.

Table 3 Acidity data of catalysts.

Catalyst	Amount of NH_3 adsorbed at different temperatures[a] (μmol/g) [a]		
	50–250 °C	250–500 °C	500–1000 °C
Dolomite	–	–	16,149
Cu/Dol	–	–	19,528
Ni/Dol	–	–	14,305
Co/Dol	–	–	11,172
Fe/Dol	–	–	6075
Zn/Dol	–	–	17,085

[a] NH_3 desorption peak for all catalysts.

3.5. Scanning electron microscopy (SEM)

Fig. 5 shows the surface morphology of all catalysts. As seen in the figures, all samples present agglomerated structure with an irregular shape of an average size of 10 mm (from scale bar), emphasizing the formation of a macroporous solid in a cluster of closely spaced crystals.

4. Catalytic hydrogenolysis performance

The glycerol hydrogenolysis reaction was carried out and the results of catalytic activity are summarized in Table 4.

A reaction without the presence of catalyst and/or support was also conducted and referred to as blank experiment. For the blank experiment, a very low glycerol conversion (8.7%) and no selectivity towards 1,2-PDO were observed. When dolomite was added, a little increase of glycerol conversion of 10.6% was observed but still no selectivity to the desired product (1,2-PDO). These results indicate that the support by itself cannot catalyze the hydrogenolysis of glycerol. A significant catalytic activity was observed on supported metal dolomite samples. Cu/Dol exhibited the highest activity in both glycerol conversion (78.5%) and 1,2-PDO selectivity (79%) among all supported metal catalysts. In contrast, Ni/Dol, Co/Dol, Fe/Dol and Zn/Dol catalysts exhibited lower glycerol conversion and 1,2-PDO selectivity of (69.5%, 52.7%), (60.9%, 58.1%), (44.8%, 5%) and (20.4%, 2.7%), respectively.

Notably, Zn/Dol showed the lowest activity of both glycerol conversion (20.4%) and 1,2-PDO selectivity (2.7%) while Ni/Dol and Co/Dol catalysts presented moderate activity in both glycerol conversion and 1,2-PDO selectivity. The trend of catalytic activity ranks as Cu/Dol > Ni/Dol ≈ Co/Dol > Fe/Dol > Zn/Dol > dolomite. A high glycerol conversion over Cu/Dol catalyst was due to its high surface acid sites. The reaction was initiated by the adsorption of glycerol on the acid sites, dehydrated and then converted to give acetol as intermediate product, and consequently yielded to 1,2-PDO. Therefore, a higher acidity provides a greater number

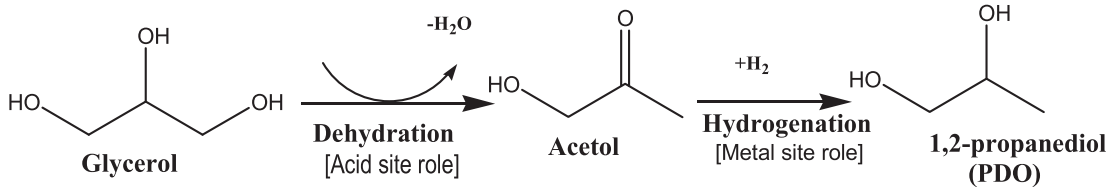

Fig. 5 SEM images of (a) Dolomite, (b) Cu/Dol, (c) Ni/Dol, (d) Co/Dol, (e) Fe/Dol and (f) Zn/Dol.

Table 4 Performance of the synthesized catalysts.

Sample	Conversion (%)	Selectivity (%)			TOF (h^{-1})
		Acetol	1,2-PDO	Methanol	
Blank	8.7	0	0	0	–
Dolomite	10.6	6.3	0	93.7	0.46
Cu/Dol	78.5	18.9	79	2.1	3.41
Ni/Dol	69.5	14.6	52.7	32.6	3.02
Co/Dol	60.9	14.2	58.1	27.6	2.65
Fe/Dol	44.8	0	5	95	1.95
Zn/Dol	20.4	0	2.7	97.2	0.89
Fe/Dol (900)	52	0	11.3	88.6	2.25
Zn/Dol (900)	22	0	5.6	94.4	0.96

Reaction conditions: 20 ml of aqueous glycerol (20 wt%); reaction temperature 200 °C; H_2 pressure 4 MPa; catalyst dosage 1 g; reaction time 10 h.

of acid sites, hence a greater number of glycerol molecules can be adsorbed on the catalyst surface (Cu/Dol) than other catalysts. This result is consistent with the literature reported that the acid site was a great influencing factor in hydrogenolysis reaction (Putrakumar et al., 2015; Yuan et al., 2009).

Apart from that, metallic site is also important for the hydrogenation of acetol intermediate to 1,2-PDO. In the case of Cu/Dol catalyst, based on the H_2-TPR profile presented in Fig. 3(A), it showed that copper species of Cu/Dol catalyst was essentially reduced at the lowest reduction temperature (291 °C) than other supported metal catalysts. According to that, the catalytic reaction conducted at 200 °C in this study is within the reduction temperature region of copper species (≥~200 °C). While for Ni/Dol, Co/Dol, Fe/Dol and Zn/Dol, the presence of respective metallic species was poor and incomplete since the reduction temperature of the catalysts occurs at higher temperature of 690 °C, 435 °C, 646 °C, and 700 °C, respectively and thus corresponded to the lower 1,2-PDO selectivity obtained by those catalysts.

For Fe/Dol and Zn/Dol catalysts, the absence of the metallic species when catalysts were reduced at 600 °C (Fig. 2(B)) was consistent with the poor activity attained by the catalysts. However, when both catalysts were reduced at 900 °C, improved activity result was obtained. This was attributed to their metal reduction behavior, of which iron and zinc oxide species was low reducible compared to copper, nickel and cobalt oxides. Apart from the formation of high 1,2-PDO product, another essential character for a good hydrogenolysis catalyst is the ability to promote high dehydration of glycerol to form acetol intermediate product and in return suppress the excess hydrogenation reaction towards side product, methanol (C-C bond cleavage). In this study, it was revealed that no selectivity towards acetol intermediate was detected for Fe/Dol and Zn/Dol catalysts. Thus, the poor selectivity towards 1,2-PDO obtained by both catalysts could be related to their incapability for producing acetol as intermediate product which subsequently hydrogenate to desired 1,2-PDO product. In addition, both catalysts also prone to catalyse C–C cleavage reaction as the selectivity towards methanol were significantly higher with 95% and 97.2%, respectively than other supported metal catalysts. Cu/Dol catalyst exhibited the lowest selectivity towards methanol (2.1%), indicating the addition of Cu to dolomite support seemed to hinder C-C cleavage reaction.

5. Conclusion

In this study, various metals supported on dolomite (Cu/Dol, Ni/Dol, Co/Dol, Fe/Dol and Zn/Dol) were synthesized for glycerol hydrogenolysis reaction and Cu/Dol catalyst was found to exhibit a promising activity when compared to other catalysts with highest glycerol conversion and 1,2-PDO selectivity of 78.5% and 79%, respectively at 200 °C of reaction temperature, 4 MPa of reaction pressure and 10 h of reaction time. The performance was attributed to its high acidity and high metal reducibility. Additionally, the reduction profile of Cu/Dol which occurred within the range of catalytic reaction temperature (at 200 °C) was important to preserve the stability of metallic Cu during catalytic reaction. The finding from this study is a valuable step in search of precious metal free and environmentally benign catalysts for the development of biomass valorization.

Declaration of Competing Interest

The authors declare that they have no known competing financial interests or personal relationships that could have appeared to influence the work reported in this paper.

Acknowledgement

The authors thank the Universiti Putra Malaysia for the Research Grant under Geran Inisiatif Putra Siswazah, GP-IPS/2018/9619500 in support of the project.

Author's contributions

All authors contributed to the success of this paper from the conception to the methodology, analysis of the results, writing proofreading, and review of the paper.

Appendix A. Supplementary data

Supplementary data to this article can be found online at https://doi.org/10.1016/j.arabjc.2021.103047.

References

Asikin-Mijan, N., Lee, H.V., Juan, J.C., Noorsaadah, A.R., Taufiq-Yap, Y.H., 2017. Catalytic deoxygenation of triglycerides to green diesel over modified CaO-based catalysts RSC Adv. 7, 46445–46460.

Bagheri, S., Muhd, N., Yehye, W.A., 2015. Catalytic conversion of biodiesel derived raw glycerol to value added products. Renew. Sustain. Energy Rev. 41, 113–127.

Balaraju, M., Rekha, V., Prasad, P.S.S., Devi, B.L.A.P., Prasad, R.B. N., Lingaiah, N., 2009. Influence of solid acids as co-catalysts on glycerol hydrogenolysis to propylene glycol over Ru/C catalysts. Appl. Catal. A : Gen. 354, 82–87.

Consonni, M., Jokic, D., Murzin, D.Y., Touroude, R., 1999. High performances of Pt/ZnO catalysts in selective hydrogenation of crotonaldehyde. J. Catal. 188, 165–175.

Freitas, I.C., Manfro, R.L., Souza, M.M.V.M., 2018. Hydrogenolysis of glycerol to propylene glycol in continuous system without hydrogen addition over Cu-Ni catalysts. Applied Catal. B, Environ. 220, 31–41.

Gallegos-Suarez, E., Guerrero-Ruiz, A., Rodriguez-Ramos, I., Arcoya, A., 2015. Comparative study of the hydrogenolysis of glycerol over Ru-based catalysts supported on activated carbon, graphite, carbon nanotubes and KL-zeolite. Chem. Eng. J. 262, 326–333.

Gandarias, I., Requies, J., Arias, P.L., Armbruster, U., Martin, A., 2012. Liquid-phase glycerol hydrogenolysis by formic acid over Ni–Cu/Al_2O_3 catalysts. J. Catal. 290, 79–89.

Kovanda, F., Jiratova, K., Rymes, J., Kolousek, D., 2001. Characterization of activated Cu/Mg/Al hydrotalcites and their catalytic activity in toluene combustion. Appl. Clay Sci. 18, 71–80.

Li, Y., Guo, Y., Xue, B., 2009. Catalytic combustion of methane over M (Ni Co, Cu) supported on ceria-magnesia. Fuel Process. Technol. 90, 652–656.

Liu, P., Derchi, M., Hensen, E.J.M., 2014. Promotional effect of transition metal doping on the basicity and activity of calcined hydrotalcite catalysts for glycerol carbonate synthesis. Appl Catal B: Environ. 144, 135–143.

Luna, F.M.T., Cecilia, J.A., Saboya, R.M.A., Barrera, D., Sapag, K., Rodríguez-Castellón, E., Jr, C.C.L., 2018. Natural and modified montmorillonite clays as catalysts for synthesis of biolubricants. Materials. 11, 1764.

Mallesham, B., Sudarsanam, P., Reddy, B.V.S., Reddy, B.M., 2016. Development of cerium promoted copper – magnesium catalysts for biomass valorization : Selective hydrogenolysis of bioglycerol. Appl. Catal. B Environ. 181, 47–57.

Mauriello, F., Vinci, A., Espro C., Gumina, B., Musolino, M. G. and Pietropaolo, R., 2015. Hydrogenolysis vs. aqueous phase reforming (APR) of glycerol promoted by a heterogeneous Pd/Fe catalyst. Catal. Sci. Technol. 5, 4466–4473.

Nagaraja, B.M.P., Seetharamulu, A.H., Reddy, P.K.H.P., Raju, B.D., Rao, K.S.R., 2007. A highly active Cu-MgO-Cr_2O_3 catalyst for simultaneous synthesis of furfuryl alcohol and cyclohexanone by a novel coupling route—Combination of furfural hydrogenation and cyclohexanol dehydrogenation. J. Mol. Catal. A: Chemical. 278, 29–37.

Pandhare, N.N., Pudi, S.M., Biswas, P., Sinha, S., 2016. Vapor phase hydrogenolysis of glycerol to 1, 2-propanediol over γ-Al_2O_3 supported copper or nickel monometallic and copper–nickel bimetallic catalysts. J. Taiwan Inst. Chem. Eng. 61, 90–96.

Pardeshi, S.K., Pawar, R.Y., 2010. Optimization of reaction conditions in selective oxidation of styrene over fine crystallite spinel-type $CaFe_2O_4$ complex oxide catalyst. Mater. Res. Bull. 45, 609–615.

Priya, S.S., Selvakannana, Komandur, P.R., Chary, V.R., Kantam, M. L., Bhargava, S.K., 2017. Solvent-free microwave-assisted synthesis of solketal from glycerolusing transition metal ions promoted mordenite solid acid catalysts. Mol Catal. 434, 184–193.

Putrakumar, B.; Nagaraju, N.; Kumar,V. P.; Chary, K.V.R., 2015. Hydrogenation of levulinic acid to valerolactone over copper catalysts supported on Al2O3. 250, 209–217.

Rajkhowa, T., Marin, G.B., Thybaut, J.W., 2017. A comprehensive kinetic model for Cu catalyzed liquid phase glycerol hydrogenolysis. Applied Catal. B, Environ. 205, 469–480.

Soares, A.V., Perez, G., Passos, F.B., 2016a. Alumina supported bimetallic Pt–Fe catalysts applied to glycerol hydrogenolysis and aqueous phase reforming. *Applied Catal.* B, Environ. 185, 77–87.

Soares, A.V.H., Salazar, J.B., Falcone, D.D., Vasconcellos, F.A., Davis, R.J., Passos, F.B., 2016b. A study of glycerol hydrogenolysis over Ru–Cu/Al_2O_3 and Ru–Cu/ZrO_2 catalysts. Journal Mol. Catal. A, Chem. 415, 27–36.

Srivastava, S., Jadeja, G.C., Parikh, Jigisha, 2017. Synergism studies on alumina-supported copper nickel catalysts towards furfural and 5-hydroxymethylfurfural hydrogenation. J. Mol. Catal. A Chem. 426, 244–256.

Tanasoi, S., Tanchoux, N., Adriana, U., Tichit, D., Sandulescu, I., Fajula, F., Marcu, I.C., 2009. New Cu-based mixed oxides obtained from LDH precursors, catalysts for methane total oxidation. Appl. Catal. A Gen. 363, 135–142.

Tasyurek, K.C., Bugdayci, M., Yucel, O., 2018. Reduction conditions of metallic calcium from magnesium production residues. Metals (Basel). 8 (383), 1–14.

Thirupathi, B., Smirniotis, P.G., 2012. Nickel-doped Mn/TiO_2 as an efficient catalyst for the low-temperature SCR of NO with NH_3: Catalytic evaluation and characterizations. J. Catal. 288, 74–83.

Vargas-Hernández, D., Rubio-Caballero, J.M., Santamaría-González, J., Moreno-Tost, R., Mérida Robles, J.M., Pérez-Cruz, M.A., Jiménez-López, A., Hernández-Huesca, R., Maireles-Torres, P., 2014. Furfuryl alcohol from furfural hydrogenation over copper supported on SBA-15 silica catalysts. J. Mol. Catal. A Chem. 383–384, 106–113.

Vasiliadou, E.S., Heracleous, E., Vasalos, I.A., Lemonidou, A.A., 2009. Ru-based catalysts for glycerol hydrogenolysis—Effect of support and metal precursor. Appl. Catal. B 92, 90–99.

Vasiliadou, E.S., Lemonidou, A.A., 2011. Investigating the performance and deactivation behaviour of silica-supported copper catalysts in glycerol hydrogenolysis. Applied Catal. A, Gen. 396, 177–185.

Wen, C., Yin, A., Cui, Y., Yang, X., Dai, W.-L., Fan, K., 2013. Enhanced catalytic performance for SiO_2–TiO_2 binary oxide supported Cu-based catalyst in the hydrogenation of dimethyloxalate. Appl. Catal. A 458, 82–89.

Xia, S., Yuan, Z., Wang, L., Chen, P., Hou, Z., 2011. Hydrogenolysis of glycerol on bimetallic Pd-Cu/solid-base catalysts prepared via layered double hydroxides precursors. Appl. Catal. A 403, 173–182.

Yan, Z., Bukur, D.B., Goodman, D.W., 2011. Silica-supported rhodium-cobalt catalysts for Fischer-Tropsch synthesis. Catal Today. 160, 39–43.

Yu, W., Zhao, J., Ma, H., Miao, H., Song, Q., Xu, J., 2010. Aqueous hydrogenolysis of glycerol over Ni–Ce/AC catalyst: Promoting effect of Ce on catalytic performance. Appl. Catal. A 383, 73–78.

Yuan, Z., Wu, P., Gao, J., Lu, X., 2009. Pt/solid-base: a predominant catalyst for glycerol hydrogenolysis in a base-free aqueous solution. Catal Lett. 131, 261–265.

Zhao, F., Li, S., Wu, X., Yue, R., Li, W., Zha, X., Deng, Y., Chen, Y., 2019. Catalytic behaviour of flame-made CuO-CeO_2 nanocatalysts in efficient co oxidation. Catalysts. 9 (3), 1–18.

Zhao, S., Yue, H., Zhao, Y., Wang, B., Geng, Y., Lv, J., Wang, S., Gong, J., Ma, X., 2013. Chemoselective synthesis of ethanol via hydrogenation of dimethyl oxalate on Cu/SiO_2: Enhanced stability with boron dopant. J. Catal. 297, 142–150.

Zhao, H., Zheng, L., Li, X., Chen, P., Hou, Z., 2020. Hydrogenolysis of glycerol to 1,2-propanediol over Cu-based catalysts: A short review. Catalysis Today. 355, 84–95.

Zhao, Y., Zhang, Y., Wang, Y., Zhang, J., Xu, Y., Wang, S., Ma, X., 2017. Structural evolution of mesoporous silica supported copper catalyst for dimethyl oxalate hydrogenation. Appl. Cat. A Gen. 539, 59–69.

Zheng, L., Xia, S., Hou, Z., 2015. Hydrogenolysis of glycerol over Cu-substituted hydrocalumite mediated catalysts. Appl. Clay Sci. 118, 68–73.

Zhu, S., Gao, X., Zhu, Y., Zhu, Y., Zheng, H., Li, Y., 2013. Promoting effect of boron oxide on Cu/SiO_2 catalyst for glycerol hydrogenolysis to 1,2-propanediol. J. Catal. 303, 70–79.